CERN - EP/79-01
2 January 1979

THE MULTISTEP AVALANCHE CHAMBER: A NEW FAMILY OF FAST, HIGH-RATE PARTICLE DETECTORS

A. Breskin*), G. Charpak, S. Majewski**), G. Melchart,
G. Petersen and F. Sauli

CERN, Geneva, Switzerland

ABSTRACT

We have investigated an unusual charge-multiplication mechanism in gases, mainly photon-mediated, that allows a controlled avalanche spread in a parallel-plate chamber. Exploiting this mode of operation, electrons can be multiplied and transferred through a succession of amplifying elements, thus constituting a multistep avalanche chamber. Several detection schemes are analysed, which provide remarkable energy, time, and position resolution both for soft X-rays and for charged particles. A gated operation of the device is described, which should allow efficient detection of particle fluxes some orders of magnitude larger than the conventional multiwire proportional chambers. Applications in several domains, such as Čerenkov ring imaging, detection of thermal neutrons, and radio-chromatography, are also discussed.

Submitted to Nuclear Instruments and Methods

---

*) On leave from the Weizmann Institute of Science, Rehovot, Israel.

**) On leave from the Institute of Experimental Physics, University of Warsaw, Poland.

1. INTRODUCTION

It has recently been shown[1] that a possible way to overcome the counting-rate limitations due to the space charge of positive ions in gas proportional counters consists in subdividing the over-all multiplication process into two steps, of which one is activated only for selected events. While the second step of amplification was performed by a conventional multiwire proportional chamber (MWPC), two methods were proposed to implement the preamplification and transfer (PAT) function, one based on secondary electron emission by low-density materials and the other relying on charge leak from a parallel-plate avalanche counter. The work on the secondary emission still being in progress at Saclay, we have at CERN concentrated our research on the second method and found results that may lead to applications far beyond the original scope of the study. In fact, a better understanding of the multiplication and transfer properties of the preamplifying element has led us to the operation of a multistep device composed only of thick wire meshes or plane grids, with suppression of the terminal MWPC element in the original design. We propose for the new device the name multistep avalanche chamber (MSC).

2. THE PREAMPLIFICATION AND TRANSFER MECHANISM

2.1 Generalities

Consider the three-electrode structure of Fig. 1, mechanically similar to the conventional MWPC design but where the applied electric field is asymmetric around the central electrode. The outer planes, a and c, are continuous conducting foils, while b consists of a closely spaced wire mesh; E_P and E_T are, respectively, the electric fields in the regions above and below the central electrode. If the electric field E_P is increased high enough to approach the inelastic collision region, electrons released in the upper region by an ionizing event develop avalanches towards the central electrode; it was observed by Fischer and co-workers[2] that some electrons from the avalanche could leak into the lower field region as a consequence of a not well understood transfer

mechanism. The observation was at the basis of the operation of the so-called hybrid chambers[3,4], where the proportional and transfer region was followed by a spark chamber that could be triggered on the delayed swarm of electrons. Similar and apparently independent observations have been made by other authors, working with d.c. spark counters[5]: in this case the avalanche multiplication in a uniform field followed by a spark chamber allowed substantial improvements in the stability of operation and in the spatial accuracy of the counter. No systematic measurements have been reported, however, on the properties and efficiencies of the PAT mechanism and the whole process remained rather mysterious. The hybrid chamber concept was eventually abandoned with the availability of relatively cheap specialized electronic circuits for the much better performing MWPC.

A quick look at the electric field structure in the vicinity of the central electrode (Fig. 2) shows the unlikelihood of a direct charge leakage from avalanches that would develop around the wires. The field lines and equipotentials have been represented for a grid of 30 μm diameter wires, 500 μm apart, and a ratio of fields E_P/E_T of five to one. There are no field lines connecting the wires to the lower field region as could be inferred from elementary electrostatics considerations [see for example Durand[6]]. If the whole of the multiplication process took place in the vicinity of the wires, for electrons to leak into the transfer region would require a path against the field of several hundred microns, which is a very unlikely process as noticed by the authors of Ref. 1. In that paper an explanation of the PAT mechanism was presented that identifies the structure shown in Figs. 1 and 2 as a parallel-plate avalanche counter, with some escaping field lines; avalanche multiplication would occur more or less uniformly across the amplification gap, and the transferred charges would correspond simply to avalanches developing along the field lines that escape into the low-field region. The measured ratio between leaking and total charges in the structure, or transfer efficiency, was consistent with the ratio of fields E_T/E_P. However, both the efficiency and the energy resolution of the counter were embarassingly good, and could be justified only by assuming a very large electron

diffusion obliterating the quantizing effect of the preamplifying grid wires. An avalanche propagation around the wires mediated by photons was disregarded as being the outcome of a direct measurement of avalanche spread in the same gas obtained with a cylindrical proportional counter with segmented cathodes[7].

2.2 Probable mechanism of the preamplification and transfer process

More detailed measurements, which we will describe in the following sections, have led us to reconsider the whole question. Although the above-mentioned diffusion-dependent transfer mechanism may actually take place, all existing evidence seems to point now towards a photon-mediated avalanche spread as a major contribution to the process. Let us briefly summarize here the observations substantiating the previous statement.

i) A careful study of localization properties for minimum ionizing particles using the structure of Fig. 1, followed by a conventional high-accuracy bi-dimensional MWPC, shows a uniform, non-modulated efficiency of detection. The preamplification gap being in this case only 3 mm thick as compared with the 0.5 mm distance between wires, an uncomfortably large value for the diffusion coefficient should be invoked to justify the results.

ii) Effective preamplification factors (inclusive of the transfer efficiency) above 200 are obtained in argon-ethanol and argon - ethanol - carbon-dioxide[1]. Use of benzene and acetone as quenching vapours considerably improves the performances of the PAT element, while trials using argon - carbon-dioxide or argon-hydrocarbon mixtures have failed owing to spark breakdown at very modest values of preamplification.

iii) Preamplification and transfer is not observed in the mixtures of xenon with any of the mentioned quenchers, unless even a small quantity of argon is added to the mixture. Full PAT behaviour appears instead in xenon quenched with triethylamine.

iv) A rather good energy resolution is observed for the transferred charge (about 17% FWHM for 5.9 keV X-rays), which is hard to justify if the PAT

process should depend only on the leak of some electrons produced in a well-localized conventional avalanche mechanism. In this case indeed the transfer yield would be expected to be strongly position dependent.

Taking into account the quoted observations, the following mechanism is suggested[8]. Electrons released in the gas by an ionizing event increase their energy in the high field region up to the point to induce secondary scintillation by inelastic collisions with the noble gas atoms. The released photons may have an energy high enough to photo-ionize the second component of the mixture efficiently, with a mean free path comparable with the grid wire distance. The very large number of photons released, combined with a good photo-ionization efficiency, explains both the good energy resolution and efficiency of the device.

Secondary light emission in pure noble gases is a well investigated phenomenon, exploited for example in gas proportional scintillation counters; an excellent review on the state of the art in this field has been given by Policarpo[9]. Detailed spectrophotometric measurements of secondary photon emission in noble gases, however, seem not to exist under the conditions we were interested in (fields around 6 kV/cm at atmospheric pressures). Proton[10] and α-particle[11] induced primary scintillation spectra have indeed been measured, as well as emission spectra using continuous or RF discharges[12,13]. They differ mainly in the shorter wavelength content as should be expected because of the different excitation energies available. Figure 3, from the work of Tanaka et al.[12], summarizes the features of the rare gas continuum obtained with the discharge method. Although the spectrum of light emission by the impact of electrons on noble gases extends from the far ultraviolet to the infrared region of the spectrum [see, for example, the review work of Thiess and Miley[14], and also Ref. 9], for the range of electric fields and pressures we are concerned with, most of the emission in argon corresponds to a broad line centred around 1250 Å (~ 9.85 eV). The measurements of Bennet and Collinson[15] show that emission around this line constitutes about 94% at low or zero electric field, increasing to 99% at fields of 4 kV cm^{-1} atm^{-1}. The RF discharge and secondary

emission spectra have been shown, using a differential filtering technique, to be comparable for xenon[16], and they correspond to a distribution centred at 1700 Å (7.3 eV) and contained between about 1550 and 1900 Å. The theory of secondary light emission is discussed in detail in Ref. 13; a recent survey of this field can be found in the work of Anderson[17].

It is assumed, in the absence of any direct information, that the main features of noble gas emission spectra remain unchanged with the addition of the mentioned quenchers, although of course the energy distribution of the electrons (and therefore the absolute value of the field at which secondary scintillation appears) can be substantially modified. The only indirect evidence of the validity of such an assumption comes from the consistency of our observations.

The photo-ionization thresholds of some quenchers used in the present study are given in Table 1 [18]. By comparison with the emission spectra shown in Fig. 3, it appears clearly that a photon-mediated amplification process can take place in argon containing benzene, acetone and (although marginally) ethanol as quenchers, while it is ineffective in argon-hydrocarbons or argon - carbon-dioxide mixtures. Only vapours with very low ionization potential, like triethylamine, can operate instead in conjunction with xenon. The photon-mediated avalanche spread will of course be more effective with quenchers having a good quantum efficiency around the noble gas emission peak; at 1250 Å, the quantum efficiency of benzene is about 60%, see Fig. 4 [19], while for acetone it is around 25%, see Fig. 5 [20]. As mentioned, addition of even small quantities of argon (1 to 2%) in a xenon-acetone mixture showed a correct PAT behaviour; we suspect this to be due to some process of energy transfer between species producing enough high-energy photons. Light emission in noble gas mixtures has been analysed by Gedanken et al.[13], but experimental data are not given for this case.

One can see from Figs. 4 and 5 that the total photon cross-section around the argon secondary emission is about 40 Mb, which implies a photon mean free path in a mixture containing a few per cent of quencher in argon, at normal conditions, of a few hundred microns. A secondary scintillation process followed by

an efficient photo-ionizing absorption at a short distance from the primary electron cluster seems to justify all previously mentioned observations. It is well known, in particular, that proportional scintillation counters, where the secondary light emission in pure noble gases or their mixtures is detected by a photomultiplier, allow the obtaining of energy resolutions approaching the limit imposed by the statistics of primary ionization [resolutions around 8.5% FWHM have been reported for 5.9 keV X-rays[21,22]]. This is due to the absence of the dispersions intrinsic in the avalanche process, which account for almost a factor of two in the obtainable resolution (see for example Curran and Wilson[23], and to the very large number of photons emitted; for a detailed discussion see the review article of Policarpo[9]. In our case, obviously, the photoemission of electrons around the primary migrating charges results in an exponential avalanche growth, very much like the conventional one, although photon-mediated; the good energy resolution obtained only implies that most or all of the primary electrons do contribute to the build-up of the fraction of charges eventually transferred to the low-field region. The quoted observation of a limited avalanche spread around the wire in a cylindrical proportional counter in the same gas mixtures (see Fig. 8 of Ref. 1) does not appear to contradict the proposed photon-mediated mechanism. In the cylindrical geometry with thin anode wires, indeed inelastic collisions begin only very close to the anode, which casts a shadow effectively limiting an avalanche spread around the wire.

It should be noted at this point that, in the high-field conditions where we are operating, the presence of a conventional charge multiplication process cannot be disregarded and may indeed contribute to the avalanche process. A direct measurement of the charge distribution in the avalanche, which has not yet been attempted, may help to understand better the relative importance of the competing processes.

We have simulated the PAT mechanism in a structure like the one of Fig. 1, using a Monte Carlo computer program. The avalanche growth induced by a single electron entering a 3 mm thick multiplication region has been reproduced,

assuming a uniform emission of a single photon at each mean free path λ followed by the generation of a new photoelectron after a (known) absorption length with the proper quantum efficiency. As an example, Fig. 6 shows a typical avalanche size, computed for 3% of acetone in argon, at an over-all charge multiplication factor of 500, experimentally observed at fields around 8 kV cm^{-1} (see Section 3.2). The quoted multiplication factor is reproduced assuming a mean free path for secondary photon emission by the electrons of about 200 μm, or a photon yield of 50 cm^{-1} per electron. Policarpo[24] estimates at 6 cm^{-1} per electron the photon yield in pure argon at normal conditions, at a field of 4 kV cm^{-1}; even considering the faster than linear light output growth in a parallel-plate geometry just above 4 kV cm^{-1} [15], a yield of 50 cm^{-1} seems rather large, and may imply the effective presence of a competing conventional charge-multiplication process. It should be noted, however, that direct absolute photon yield measurements in scintillating proportional counters do not exist, the quoted values depending on the proper estimate of several large inefficiency sources; for example, Anderson[17] has suggested an underestimation of the photon yield in xenon by a factor as large as 10 to justify his measurements (see p. 72 of Ref. 17).

As expected, the amount of quencher controls the avalanche lateral spread, but has almost no influence on the charge gain. The simulation program has been used also to estimate the energy and position resolution in the detection of both X-rays and charged particles, as will be discussed in the following sections.

3. DEVELOPMENT OF THE MULTISTEP AVALANCHE CHAMBER

3.1 Construction schemes

The basic PAT element of Fig. 1 has been used to implement several chamber geometries, some of which are schematically shown in Fig. 7. Figure 7a corresponds to the original construction as described in Ref. 1; a drift and conversion region is followed by a PAT element and then by a conventional MWPC.

This scheme has been used mainly to study the properties of the preamplification process, since it allows good energy resolution to be obtained on soft X-rays. The first drift field can be inverted, limiting the detection only to charges produced in the high-field part of the PAT element (in fact, only to electrons liberated close to its upper grid); this mode of operation has been used mainly to study the efficiency and localization properties for minimum ionizing tracks. Bi-dimensional localization in the MWPC can be obtained recording, event per event, the induced positive charge distribution on the cathodes properly stripped, a method that is known to provide very good accuracies of reconstruction[25].

In Fig. 7b two parallel-plate elements are mounted in cascade, constituting a true MSC; this scheme allows very good time resolutions on charged particles to be obtained, as compared with the situation with a conventional MWPC, the major source of dispersion (the large anode wire spacing) being greatly reduced.

Figure 7c shows instead a PAT element followed by a pair of fine wire meshes, allowing an electronic gating of the preamplified electron cluster following the principles described in Ref. 1. Only selected tracks are let through the gate and receive the full amplification, thus greatly improving the rate capability of the detector; localization is again performed in a bi-dimensional MWPC.

In all cases, several electrode configurations have been tried, both with parallel wire grids or crossed wire meshes; it appears that there are not major differences in the PAT behaviour, as far as the central electrode has a fine enough structure. Most of the results described hereafter have been obtained with electrode a (see Fig. 1) consisting either of a thin aluminium foil or a mesh of crossed stainless steel wires, 0.1 mm thick and with 85% optical transparency; electrode b, on the other hand, has been implemented with the same kind of mesh, or with a grid of parallel, 30 to 50 μm diameter wires at 500 μm as in the original design[1]. Preamplification gaps between 3 and 5 mm have been used, followed by a transfer region 5 to 20 mm thick depending on the application. Notice that rather stringent mechanical tolerances are required on the preamplification gap thickness, since a 3% change in the gap results in about a factor of two gain variation (see the next section).

As in conventional parallel-plate counters, precautions should be taken to avoid breakdown at the edges of the frame; we have used either graded potential guard rings or thin insulator sheet insets around the edges.

3.2 Experimental results: preamplification factor

Addition of an absorption and drift region to any of the PAT structures allows a good energy resolution to be obtained on electrons photoproduced in the upper space and subsequently multiplied. When studying the multiplication factor, one should of course distinguish between the total charge gain in the PAT element and the fraction of charges transferred to the lower element, or effective preamplification: the ratio of the two is simply the electron transparency of the middle wire grid or mesh. We have directly measured the transparency of electrode b (see Fig. 1) as a function of E_T/E_P, recording the ion currents in all electrodes at a constant irradiation flux. The results are summarized in Fig. 8, where the measured electron transparency is shown for two electrode constructions, i.e. a 50 μm diameter, 500 μm spacing parallel wire grid (full points) and a crossed wire mesh with 85% optical transparency (open circles). The broken line represents the computed transparency in the first case, following Buneman et al.[26], for a uniform distribution of charges; the good matching with the experimental results proves that the photon-mediated avalanche spread is very effective in obliterating the wire structure (as discussed in Section 2.2). It appears that a stable operation can be obtained operating the PAT element at transfer efficiencies between 20 and 30%; in this region, the transparency is essentially equal to the fields ratio.

When the chamber shown in Fig. 7a is exposed to a soft X-ray source and the preamplification field E_P is increased (keeping E_T constant), at a threshold value for E_P, the preamplified signal, detected on the MWPC anode and corresponding to electrons photoproduced in the upper region, separates from the signal due to charges liberated either in the transfer region or in the MWPC itself (hereafter referred to as direct signal). Figure 9 shows this behaviour, at increasingly high values of E_P, obtained for the 5.9 keV line in argon-ethanol

(98-2). The ratio between the preamplified and the direct pulse heights provides the value of the effective preamplification, and correction by the transfer efficiency (Fig. 8) allows estimation of the real charge multiplication of the PAT element. A measurement of the effective preamplification factor as a function of E_p for a transfer efficiency around 10%, obtained under the same conditions, is shown in Fig. 10, at a constant transfer field E_T; the corresponding total multiplication factor is also given in the figure. Similar curves have been measured using benzene and acetone as quenchers, always in the few per cent volume content range; acetone seems to provide a better stability of operation and breakdown protection, at effective preamplification factors of several hundreds. Obviously, in the region of fields where we are operating, discharge or spark breakdown constitute the ultimate limits in the obtainable gains, and small differences in the properties of the addition to absorb hard photons and to quench metastable atoms may play a major role. It should be noted in this context that the MWPC operating in the same gas mixture enters a full Geiger régime at charge gains around 10^4; when using a PAT structure in conjunction, however, combined gains above 10^6 can be obtained still in a proportional or semi-proportional régime. The explanation of this somehow surprising behaviour resides in the fact that photons released in the final avalanche, whose reconversions in the gas are responsible for the Geiger spread at large gains, are mostly reabsorbed within the MWPC volume and produce therefore an avalanche size below the critical. This is true for all described multistep structures, as far as the distance between the two amplifying elements is sufficiently large (compared to the photon absorption length), thus explaining why over-all gains can be obtained that are not allowed in a single element.

As indicated in Section 2.2, the PAT mechanism has been observed in xenon coupled with triethylamine, having an ionization potential (7.5 eV) matching its secondary emission spectrum, but also using a quencher with higher ionization potential (as acetone) if small quantities of argon are added into the mixture. We have also verified that the PAT mechanism remains effective in a 80-20 mixture

of argon and xenon (with the addition of 2% acetone); this observation is relevant for all cases where good efficiency of detection for soft X-rays is demanded, without the economic implications of using xenon alone; in the indicated mixture the absorption mean free path for 8 keV X-rays is around 20 mm, as compared to 50 mm for pure argon.

At large preamplifications, a charge signal can be detected directly on the electrodes of the preamplification gap, as shown in Fig. 11 for ^{55}Fe X-rays. In both pictures, a charge amplifier with 1 μsec decay time was used; for a given preamplification field, the pictures show, respectively, the detected signal in case of no electron transfer ($E_T = 0$, Fig. 11a) and of about 30% transfer ($E_T/E_P \simeq 0.32$, Fig. 11b). While the first image has the typical parallel-plate chamber characteristics, the second shows clearly the contribution of the electrons drifting away from the grid; although the number of transmitted electrons is about a third of the total, they induce a large positive signal all along their drift to the next electrode (5 mm apart in this case). The contribution of the positive ions migrating in the preamplification gap is also visible.

3.3 The multistep avalanche chamber

As shown in Fig. 10, rather large charge multiplication factors can be obtained in the preamplification gap. It is therefore conceivable that two parallel-plate elements in cascade, of which the first operated in the PAT mode and the second in the usual multiplication and collection mode can reach gains up to 10^5, convenient for electronic detection. The chamber illustrated schematically in Fig. 7b has therefore been constructed and tested with a conversion and drift attachment for the X-ray studies. The two amplification gaps were 3 mm thick with a 5 mm long transfer region in between.

Amplification curves obtained in argon-acetone for the 5.9 keV line detected on the last electrode are shown in Fig. 12; it appears that spark breakdown limits the over-all multiplication factor of the combined structure (broken curve in the figure). Below this limit, one can vary the gains of the two elements

independently. The described structure, that constitutes a true MSC allows the best energy and time resolutions to be obtained. Figure 13 shows the signal and the corresponding pulse-height distribution as detected on the last electrode at an over-all gain of around 10^4 for ^{55}Fe X-rays, and having about 17% FWHM for the 5.9 keV line; we believe that with a more careful mechanical construction of the chamber, to ameliorate its uniformity of response, the energy resolution can further be improved.

Considering that the major source of time jitter in the detection of charged particles by conventional MWPCs is due to their discrete anode wire spacing, one expects a MSC to provide a superior time resolution. In fact, time resolutions of a few hundred picoseconds have been obtained in parallel-plate avalanche chambers in the detection of heavily ionizing light particles[27]. In our case, obviously, both the time and the pulse-height jitters of the detected signal will be dominated by the statistical fluctuations in the position of the ion pair produced further away from the first preamplification electrode. The best result obtained so far, using the two-step structure of Fig. 7b (without the drift and conversion attachment) operated in argon-acetone (97-3), in the detection of minimum ionizing electrons is shown in Fig. 14; the distribution has a FWHM of 9 nsec (1.5 nsec/channel). This result has been obtained with a simple threshold operated fast discriminator, certainly not very suitable because of the relatively slow rise-time of the detected pulse ($\sim$ 30 nsec), characteristic of a parallel-plate chamber operation.

3.4 Detection and localization of minimum ionizing particles

We have analysed the efficiency and localization properties of the MSCs in the detection of minimum ionizing charged particles, mostly using the structure illustrated in Fig. 7a with the second element (the MWPC) equipped with a bi-dimensional read-out based on the centre-of-gravity calculation of the induced charge[25,28]. Both the schemes with and without a conversion and drift attachment were tried, since they present distinct advantages. In the first case a good efficiency and energy resolution can be obtained, the device providing a uniform gain for all charges liberated in the conversion space, rapidly falling

off for the charges produced within the preamplification volume. In the second case instead there is essentially no energy resolution, since the detected pulse height is dominated by the statistical fluctuations in the position of the primary charges in the preamplification region; indeed, the mean free path for secondary photon emission, Section 2.2, is comparable with the average distance of primary clusters produced by minimum ionizing particles (around 300 μm). On the other hand, one expects to obtain in this case a better time resolution and a shorter physical extension of the transferred electrons, essential parameters in view of the use of the device in the gated mode as in the original design.

From the beam measurements it appears that, using an electronic discrimination threshold around 0.1 pC, a 3 mm thick preamplification region is not sufficient to provide full efficiency of detection for minimum ionizing particles, when the conversion and drift space is omitted, for the reasons indicated. As shown in Fig. 15a, however, addition of a 5 mm thick conversion space is sufficient to restore full efficiency of detection. Alternatively, one can use a thicker preamplification volume, thus reducing the dependence of the detected pulse height on the statistical distribution of the primary clusters since, for a given charge gain, the mean free path for multiplication is correspondingly increased; Figure. 15b shows the behaviour of a chamber having 5 mm thick preamplification, with and without the drift and conversion attachment.

As mentioned in Section 2.2, analysis of the localization properties for minimum ionizing particles of the MSC has added an essential piece of information to help our understanding of the PAT mechanism. It appears indeed that even in the case of limited detection efficiency (lower curve in Fig. 15a) the inefficiency is uniformly distributed across the preamplifying wire structure, this ruling out any explanation of the PAT mechanism based on a preferential avalanche formation and leak around the wires, and implying an avalanche spread far too large to be only imputed to electron diffusion. The MSC under test was mounted in a high-energy charged particle beam between two conventional MWPCs, and coordinate localization was obtained measuring event per event the induced charge

distribution on the cathode planes of each chamber; typically 50 nsec gating times were used in time coincidence with the preamplified and delayed charge for the central chamber. As was known from previous work done in our group with the same read-out, localization accuracies well below 100 μm can be obtained in the normal case (conventional MWPCs operating at large gains in argon-isobutane mixtures) in the measurement of the coordinate parallel to the anode wires[28]. The MSC was therefore mounted such that the best measured coordinate was in the direction perpendicular to the preamplification grid wires. Using the two other chambers as a reference, both the absolute coordinate and the accuracy in the MSC could be measured; Fig. 16 shows the average deviation from a linear response as measured in the MSC, as a function of position along the coordinate perpendicular to the preamplifying wires: a modulation having 500 μm wavelength (the wire spacing) clearly appears, with a full amplitude not exceeding 60 μm. The effect is understood as being a consequence of the selective extraction of electrons from the PAT mechanism, taking into account that the avalanche spreads only across three or four wires. One would, of course, expect the modulation to be reduced with lower quencher concentrations, owing to the more effective photon-mediated avalanche spread; this has indeed been observed experimentally. The continuous curve in Fig. 16 represents a fit to the simulation of the process realized using the previously described Monte Carlo program (Section 2.2).

Figure. 17, curve b, shows the projected accuracy distribution, always in the direction perpendicular to the preamplifying wires, obtained as a simple difference of coordinates. Comparison with the same distribution measured with three identical conventional MWPCs (curve a) allows the computation of a standard deviation for the accuracy given by the chamber with preamplification $\sigma_{PA} \simeq 100$ μm as compared to the normal value $\sigma_N \simeq 70$ μm. Assuming independent contributions, one can attribute to the PAT mechanism an intrinsic dispersion when detecting charged particles of around 70 μm; this includes the previously described modulation effect.

3.5 Gated operation of the multistep avalanche chamber

Operation of a gated multistep device was the original motivation for investigating the PAT mechanism. According to the authors of Ref. 1, indeed, the following scheme can be implemented (Fig. 18). A preamplification element A_1 of effective gain M_1 is followed by an electronic gate G that selectively (under control of external potentials) transmits or stops electrons extracted from A_1; in case of transmission, the lower amplification element A_2, of gain M_2, allows an over-all multiplication factor $M = M_1 M_2$ to be obtained, sufficient for efficient detection. For an operation where the selected events rate is negligible in respect to the total particle flux, the number of positive ions liberated at the anode of the chamber A_2 is reduced by a factor M_1. Since the pulse-height reduction in a proportional counter due to the positive ion space charge is roughly proportional to e^{-MR} [where R is the particle flux[29)]], for $M_1 \simeq 100$ one expects to improve the rate capability of the device by two orders of magnitude.

The gating function has been tried in a 10×10 cm^2 useful surface MSC containing an electronic shutter, following the scheme of Fig. 7c. With a drift- and conversion-space attachment, charges produced by soft X-ray photoelectrons could be preamplified and detected in the PAT element, so as to provide a time reference for the application of the gating pulse to the double mesh structure G. The d.c. electric fields in the structure were arranged such that either full transmission or full blocking could be obtained for electrons traversing the gate G; for the mesh distance chosen (3 mm) a forward difference of potential around 70 V (d.c. or pulsed) was necessary for full transparency, while a few volts of reverse bias were enough for complete blocking. Figure 19 shows the signal on the lower anode plane, when detecting the preamplified and delayed electron swarm with a forward d.c. bias (upper trace), and with a timed pulse opening of the otherwise reversely biased gate (lower trace). A large pick-up signal appears on the anodes in the second case because of the capacitive coupling between the gate meshes and the anodes, but the time difference between the spurious and the real signal, determined by the drift-time in the second transfer region T2 and in the

MWPC, is sufficient for full separation. Clearly capacitive pick-up constitutes the major problem in the scheme described, especially for large surface chambers. In our case, although the chamber surface was only 100 cm^2, all wires in the anode plane were connected together on the amplifier input thus reproducing the conditions of a chamber of much larger size (for any practical case, individual or grouped wire read-out is necessary to achieve localization).

The system has so far not been tried in real operational conditions; all evidence, however, suggests that it should perform as expected and allow efficient detection of selected tracks in a very large particle flux.

3.6 Single electron detection and Čerenkov ring imaging

Over-all charge gains in excess of 10^6 could be obtained in the combined structure illustrated in Fig. 7a. For a single electron, photoproduced within the conversion and drift space, this corresponds to a total charge of about 1 pC, that can be detected using inexpensive charge amplifiers*). As an example, Fig. 20 shows a pulse-height distribution as measured on the anode of the MWPC for single electrons photoproduced on the upper cathode of the MSC by an ultraviolet lamp. A peak appears clearly over noise, thus confirming that single-electron detection and localization (e.g. by the induced charge method) can be achieved. The first immediate application of the device appears therefore in Čerenkov ring imaging. The possibility of identifying charged particles emitted in large angular spreads and multiplicities through reconstruction of the diameter of the Čerenkov light cones, projected on an image plane by suitable optics, has been known for a long time. Only recently, however, it has been recognized that since photon emission in the process extends towards short wavelengths, in the far ultraviolet region where many gases and vapours exhibit a large quantum efficiency, it is worth using gaseous imaging devices[30]. It appears that suitable combinations of window materials and photosensitive gases can provide quantum

*) For most of our measurements, we have used a charge amplifier developed at CERN by J.C. Santiard and produced in a thick-film hybrid technology by CIT-Alcatel, France.

efficiencies in excess of 60% above ionization threshold; the problem, however, is to get enough gaseous gain for single-electron detection in a proportional device having, by definition, very poor photon quenching properties. Multiwire proportional chambers allow, in fact, gains to be reached in excess of 10^6 (10^7 can be obtained using the so-called magic gas), but this is obtained using gas mixtures that highly quench the propagation of the photons, responsible for the Geiger discharge or breakdown with non-ionizing absorption or, in other words, having a very small quantum efficiency. Attempts have been made recently to use MWPCs in poorly quenched gas mixtures, but so far single-electron detection has not been obtained with reasonable efficiencies[31-33].

We have simulated a Čerenkov ring image using a mask in front of our MSC, and illuminating the device with an ultraviolet lamp. At a low detection threshold on the MWPC anode, a bi-dimensional reconstruction of the coordinates of each detected photon could be made using the previously described centre-of-gravity read-out; a typical image obtained in a short run is shown in Fig. 21. The mask ring diameter and thickness are 40 and 1 mm, respectively; scattered points correspond to background counts. Notice that, contrary to an effective use, the device was in this case completely ungated, essentially recording any event during the running time (about 2 min).

In the real case, obviously all photons emitted by the charged particle reach the detector at the same time, thus requiring a more sophisticated read-out method. We are investigating both the possibility of using multilayer wire structures, oriented at different angles and successively traversed by the electron swarms, or of adopting a true bi-dimensional read-out method consisting of a dense matrix of electrodes or pads. The use of MWPCs having on each wire a coordinate localization based on the current division method[34] may also be possible, although multiple hits on the same wire would not properly be reconstructed.

4. CONCLUSIONS AND FUTURE PROSPECTS

We have shown that it is possible to multiply electrons, and to transfer them efficiently and uniformly into a succession of gaps in order to obtain a variety of functions. All electrodes in such a structure can be made either with wires or meshes, thus eliminating one major source of breakdown in large detectors. The large gains, good accuracies, and time resolutions that can be obtained with the MSCs allow their use in all applications where MWPCs have been used so far, but with a rate capability (in the gated version) at least two orders of magnitude higher for selected events. However, some new applications are allowed by the specific properties of the MSC:

i) In conjunction with a conventional bi-dimensional localization method based on the induced charge read-out, the MSC offers an internal gaseous delay of several hundred nsec that can be exploited to gate the information selectively in a set of analog-to-digital converters (ADCs), without the need for electronic delays (usually implemented by cumbersome coaxial cables). The appearance on the market of inexpensive and fast monolithic ADCs would seem to allow the design of centre-of-gravity digital electronics fully integrated directly on the chamber wire planes.

ii) The single-electron detection allows applications to be foreseen in the ultraviolet and Čerenkov radiation imaging, where the velocity of relativistic particles is measured from the opening of the emitted light cone. As a matter of fact, the principle itself of the PAT process demands the use of a gas with very efficient photoelectric conversion at ultraviolet wavelengths, where a large fraction of Čerenkov light is emitted.

iii) In radio-chromatography applications, the parallel-plate characteristics of the preamplifying gap should ensure a good localization accuracy, despite the long range of emitted electrons, since the largest avalanche starts from the entrance point in the gap of the electrons.

iv) For slow neutron detection, the use of a conversion foil with a large cross-section, for example made of gadolinium, as the first electrode, should, for the same reasons, allow very good localization.

v) In spherical drift chambers[35] a preamplifying gap at the end of the drift space should permit selection of X-ray conversion taking place within the drift space, thus in some cases eliminating the need for using xenon to reduce the background of photons converted in the transfer space or in the MWPCs.

Acknowledgements

We are indebted to A. Policarpo and T. Ypsilantis for useful discussions on the gaseous mechanism discussed in this article. Most of our work has benefited from the technical assistance of R. Bouclier, G. Millon and J.C. Santiard.

REFERENCES

1) G. Charpak, G. Melchart, G. Petersen, F. Sauli, E. Bourdinaud, P. Blumenfeld, J.C. Duchazeaubeneix, A. Garin, S. Majewski and R. Walczak, New approaches in high-rate particle detectors, CERN 78-05 (1978).

2) J. Fischer and S. Shibata, Proc. Internat. Symposium on Nuclear Electronics, Versailles, 1968 (Documentation Française, Paris, 1969), Vol. 3, p. 2-1.

3) J. Fischer and S. Shibata, Nuclear Instrum. Methods 401, 157 (1972).

4) V. Bohmer, Nuclear Instrum. Methods 107, 157 (1977).

5) T. Aoyama and T. Watanabe, Nuclear Instrum. Methods 150, 203 (1978).

6) E. Durand, Electrostatique (Masson, Paris 1966), Vol. 3, p. 69.

7) G. Charpak, G. Petersen, A. Policarpo and F. Sauli, IEEE Trans. Nuclear Sci. NS-25, 122 (1978).

8) G. Charpak and F. Sauli, Physics Letters 78B, 523 (1978).

9) A.J.P. Policarpo, Space Science Instrum. 3, 77 (1977).

10) T.E. Stewart, G.S. Hurst, T.E. Bortner, J.E. Parks, F.W. Martin and H.L. Weidner, J. Opt. Soc. Amer. 60, 1290 (1970).

11) T.D. Strickler and E.T. Arakawa, J. Chem. Phys. 41, 1783 (1969).

12) Y. Tanaka, A.S. Jursa and F.J. Le Blanc, J. Opt. Soc. Amer. 48, 304 (1975).

13) A. Gedanken, J. Jorten, B. Raz, and A. Szöke, J. Chem. Phys. 57, 3456 (1972).

14) P.E. Thiess and G.H. Miley, IEEE Trans. Nuclear Sci. NS-21, 125 (1974).

15) J.R. Bennet and A.J.L. Collinson, J. Phys. B 2, 571 (1969).

16) R.D. Andresen, E.A. Leiman and A. Peacock, Nuclear Instrum. Methods 140, 371 (1977).

17) D.F. Anderson, A high resolution large area gas scintillation proportional counter for use in X-ray astronomy, Ph.D Thesis, Columbia University, New York (1978).

18) Handbook of Chemistry and Physics (ed. R.C. Weast) (The Chemical Rubber Co, Cleveland, 1970).

19) J.C. Person and P.P. Nicole, ANL-7760 (1970).

20) J.C. Person, J. Chem. Phys. 43, 2553 (1965).

21) A.J.P. Policarpo, M.A.F. Alves, M.C.M. Dos Santos and M.J.T. Carvalho, Nuclear Instrum. Methods 102, 337 (1972).

22) H.E. Palmer and L.A. Braby, Nuclear Instrum. Methods 116, 587 (1974).

23) S.C. Curran and H.W. Wilson, Proportional counters and pulse ion chambers in alpha-, beta- and gamma-ray spectroscopy (ed. K. Siegbahn), (North-Holland, Amsterdam, 1965), Vol. 1.

24) A.J.P. Policarpo, Nuclear Instrum. Methods 153, 389 (1978).

25) G. Charpak, G. Petersen, A.J.P. Policarpo and F. Sauli, Nuclear Instrum. Methods 148, 471 (1978).

26) O. Bunemann, T.E. Cranshaw and J.A. Harvey, Canad. J. Research 27A, 191 (1949).

27) A. Breskin and N. Zwang, Nuclear Instrum. Methods 144, 609 (1977).

28) G. Charpak, G. Melchart, G. Petersen and F. Sauli, High accuracy localization of minimum ionizing particles using the induced charge centroid read-out method, in preparation.

29) R.W. Hendricks, Rev. Sci. Instrum. 40, 1216 (1969).

30) J. Seguinot and T. Ypsilantis, Nuclear Instrum. Methods 142, 377 (1977).

31) J. Chapman, D. Meyer and R. Thun, VM HE 78-23, Submitted to Nuclear Instrum. Methods (1978).

32) R.S. Gilmore, J. Malos, D.J. Bardsley, F.A. Lovett, J.P. Melot, R.J. Tapper, D.I. Giddings, L. Lintern, J.A.G. Morris, P.H. Sharp and P.D. Wroath, An observation on the spatial distribution of vacuum UV photons generated by Čerenkov radiation, University of Bristol preprint (July 1978).

33) S. Durkin, A. Honma and D.W.G.S. Leith, SLAC-PUB-2186 (1978).

34) V. Radeka, IEEE Trans. Nuclear Sci. NS-21, 51 (1974).

35) G. Charpak, C. Demierre, R. Kahn, J.C. Santiard and F. Sauli, Nuclear Instrum. Methods 141, 449 (1977).

Table 1

Photo-ionization thresholds of some quenchers used in the present study

		Ionization potential (eV)
CO_2	Carbon-dioxide	13.77
CH_4	Methane	12.6
C_2H_6	Ethane	11.5
C_2H_5OH	Ethanol	10.49
CH_3COCH_3	Acetone	9.69
C_6H_6	Benzene	9.24
$(C_2H_5)_3N$	Triethylamine	7.50

Figure captions

Fig. 1 : Schematics of the gaseous PAT element. A region of high electric field E_P is followed by a lower field E_T; the electrode b can be either a parallel wire grid (as represented) or a crossed wire mesh. Under the conditions described in the text, charge multiplication may take place in the upper region with a considerable electron leakage into the lower one.

Fig. 2 : Detailed structure of the electric field equipotentials and field lines around the central electrode of the PAT structure, computed for 30 μm diameter wires, 500 μm apart at a ratio of fields $E_T/E_P \simeq 0.2$.

Fig. 3 : Schematic representation of the rare-gas photon emission continua [from Tanaka et al.[12)]].

Fig. 4 : Absorption cross-section σ_T and quantum efficiency η as a function of photon energy for benzene[19)].

Fig. 5 : Absorption cross-section σ_T and quantum efficiency η as a function of photon energy for acetone[20)].

Fig. 6 : Computer simulation of the photon-mediated avalanche spread in a parallel-plate chamber. The calculation has been made for a 3 mm thick gap operated in argon-acetone (97-3) at atmospheric pressure, taking into account the known values of the total and photo-ionization cross-section at the argon secondary emission line (9.85 eV), as from Fig. 5. To reproduce an experimentally observed total multiplication factor of 500 a mean free path for secondary photon emission by electrons of about 200 μm is required. Conventional charge multiplication, by direct electron impact ionization, is neglected in this model.

Fig. 7 : Several kinds of MSCs that have been implemented for the purposes of the present experimental work:

a) A PAT element followed by a conventional MWPC; addition of a conversion and drift space allows injection into the amplifying sections of a known amount of charges (X-ray photoconversions). This structure has been used mainly to study the preamplification factors and the energy and position resolution both for X-rays and charged particles.

b) Two parallel-plate elements, with a transfer of charge from PA1 to PA2. The best energy and time resolutions have been obtained using this configuration.

c) A gated MSC, where a pair of closely spaced electrodes (G in the figure) control the transmission of electrons from the PAT element to the MWPC. Transmission may be either d.c. or pulse operated, the last in view of a high-rate operation of the element.

Fig. 8 : Measured electron transparency as a function of the ratio of the fields of the central electrode of the PAT structure (electrode b in Fig. 1), implemented either with a grid of wires 50 μm in diameter, 500 μm apart (full points), or with a crossed wires mesh, 85% optical transparency (open circles). The dashed curve is a calculation of transparency for the first case, taken from Buneman et al.[26].

Fig. 9 : Observation of the detected signal on the anodes of the MWPC (see Fig. 7a) for a uniform iradiation with an ^{55}Fe X-ray source. Above threshold value for the field E_p, the preamplified and the direct signals separate, and their ratio gives the value of the effective preamplification factor, as shown in the figures for a preamplification factor of 4 and 25, respectively. Horizontal scale 1 μsec/div.

Fig. 10 : Effective (M_E) and total (M_T) preamplification factors as measured in the PAT structure operated in argon-acetone (97-3), as a function of the preamplification field E_P at a constant transfer field. The transfer efficiency for this case (see Fig. 8) is around 10%.

Fig. 11 : Detection of charge signals directly on the electrodes of the preamplification gap. For a PAT element operating in argon-acetone at a total amplification factor of around 500, the signal produced by 5.9 keV X-ray photoelectrons is shown for the case of no electron transfer ($E_T = 0$, Fig. 11a), and for about 30% transfer efficiency ($E_T/E_P \simeq 0.32$, Fig. 11b). The effect of the electrons drifting away from the signal electrode is clearly visible in the second picture.

Fig. 12 : Charge multiplication factor measured in the MSC of Fig. 7b, as a function of the difference of potential across the two amplifying elements PA1 (V1) and PA2 (V2), 3 mm thick each, at a constant field in the transfer region T (1 kV over 5 mm). Gas filling: argon-acetone 97-3.

Fig. 13 : a) Charge signal detected on the second element of the MSC (lower electrode of PA2, Fig. 7b) for ^{55}Fe 5.9 keV X-rays at an over-all gain around 10^4 (horizontal scale 50 nsec/div.), and b) the corresponding pulse-height distribution.

Fig. 14 : Time resolution of the MSC measured on the lower electrode of the structure shown in Fig. 7b for fast electrons (time reference given by external scintillation counters). The horizontal sensitivity corresponds to 1.5 nsec/channel, and the distribution has 9 nsec FWHM.

Fig. 15 : Efficiency for detection of minimum ionizing particles of the MSC. The structure of Fig. 7a has been used with or without the upper conversion and drift attachment.

a) Preamplification gap 3 mm thick, with and without a 5 mm thick conversion and drift region (dashed and full curves, respectively). The efficiency at a fixed threshold ($\sim$ 0.1 pC) has been measured as a function of the preamplification difference of potentials V_1 at a fixed MWPC anodic potential (V_2 = 1.5 kV).

b) Preamplification gap 5 mm, with and without a 10 mm conversion region (dashed and full curves, respectively). In this case, full efficiency is obtained also without the conversion attachment.

Fig. 16 : Modulation in the coordinate measurement for minimum ionizing particles in the direction perpendicular to the preamplifying wires (points with error bars). The wavelength of the modulation corresponds to the wire spacing (500 μm), and the maximum amplitude does not exceed 60 μm. The full curve represents a fit to the Monte Carlo simulation of the photon-mediated PAT mechanism.

Fig. 17 : Projected accuracy distribution for the localization of minimum ionizing particles in the direction perpendicular to the preamplifying wires, obtained as the difference of coordinates in a set of three parallel chambers with a centre-of-gravity read-out method. The dashed curve (curve a) represents the result obtained with three conventional MWPCs; as indicated in the figure, the distribution has a standard deviation of 85 μm, or 70 μm per chamber. Curve b, instead, has been measured replacing the central chamber with a MSC (as in Fig. 7a, without the drift and conversion attachment); by subtraction, one can obtain $\sigma_{PA} \simeq 100$ μm as shown.

Fig. 18 : Principle of gated multistep detector[1]. The amplification M_2 of the MWPC A_2 is decreased by a factor M_1 with respect to normal gain $M = M_1 \cdot M_2$. The electrons liberated in the gap A_1 are preamplified

by a factor M_1 and then transferred to A_2, after drifting in the space D, under the control of the gate G. Conditions are set such that A_2 detects only the preamplified electron bunch. The electronic gate G opens only for preselected events; if their number is much smaller than the over-all particle flux, the space-charge reduction is roughly equal to M_1.

Fig. 19 : Operation of the gated MSC, see Fig. 7c. The upper oscilloscope trace shows the signal detected on the anode in conditions of full transparency of the gate G (d.c. forward biased), for X-ray conversion in the upper structure; the lower trace shows instead a timed pulsed opening of the gate, otherwise reverse biased. The time reference for the scope triggering and the gate pulse generation is provided by the signal detected on the PAT element. Horizontal scale 1 μsec/division.

Fig. 20 : Pulse-height distribution for single electrons, photoproduced on the upper cathode of the MSC of Fig. 7a by an ultraviolet lamp. The peak in the distribution, measured in argon-acetone 97-3, corresponds to a detected charge of around 1 pC.

Fig. 21 : Simulated Čerenkov ring image, obtained by exposing the MSC with bi-dimensional read-out to an ultraviolet lamp source through a ring mask, 40 mm in diameter with a width of 1 mm. Scattered points correspond to background counts during the running time of around 2 min.

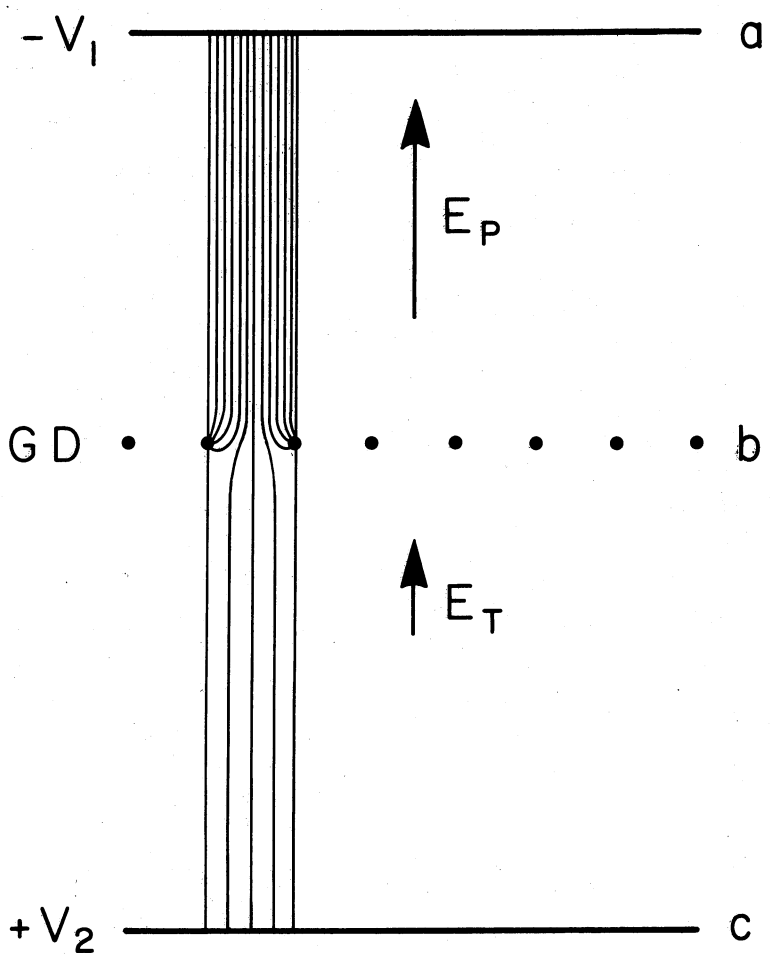

Fig. 1

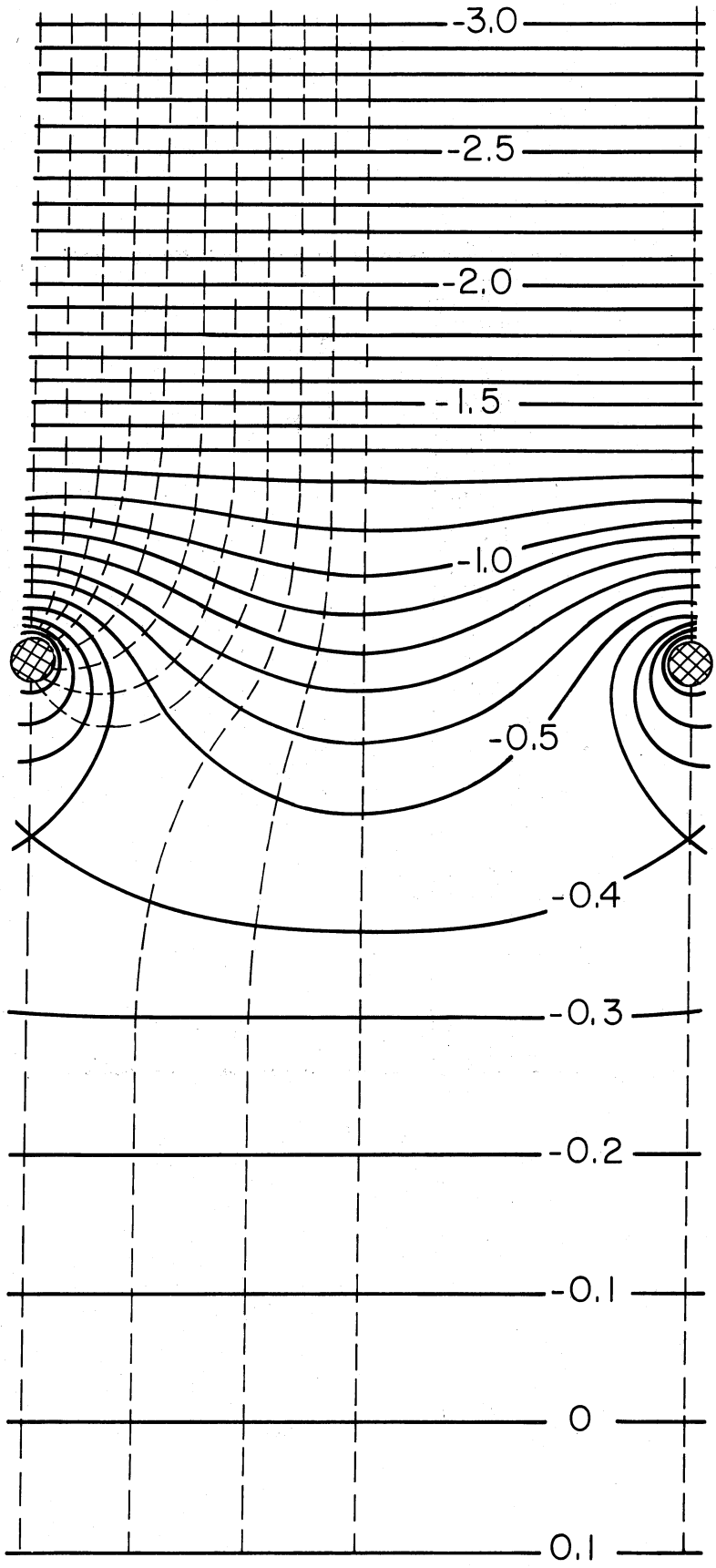

Fig. 2

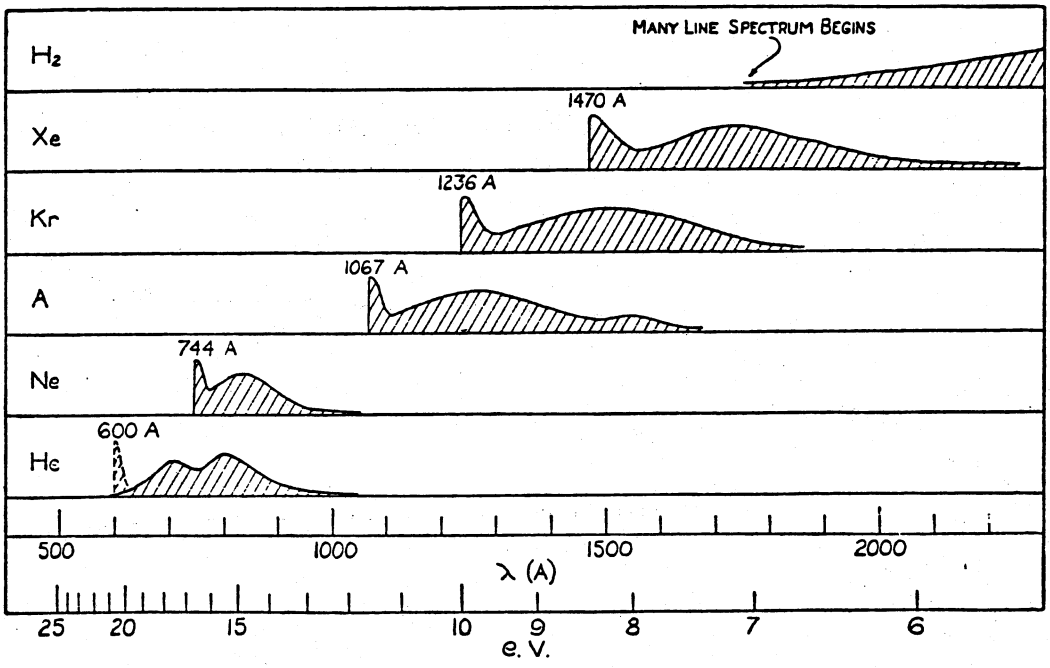
MANY LINE SPECTRUM BEGINS
H₂
1470 A
Xe
1236 A
Kr
1067 A
A
744 A
Ne
600 A
He
500
1000
1500
2000
λ (A)
25
20
15
10
9
8
7
6
e.V.

Fig. 3

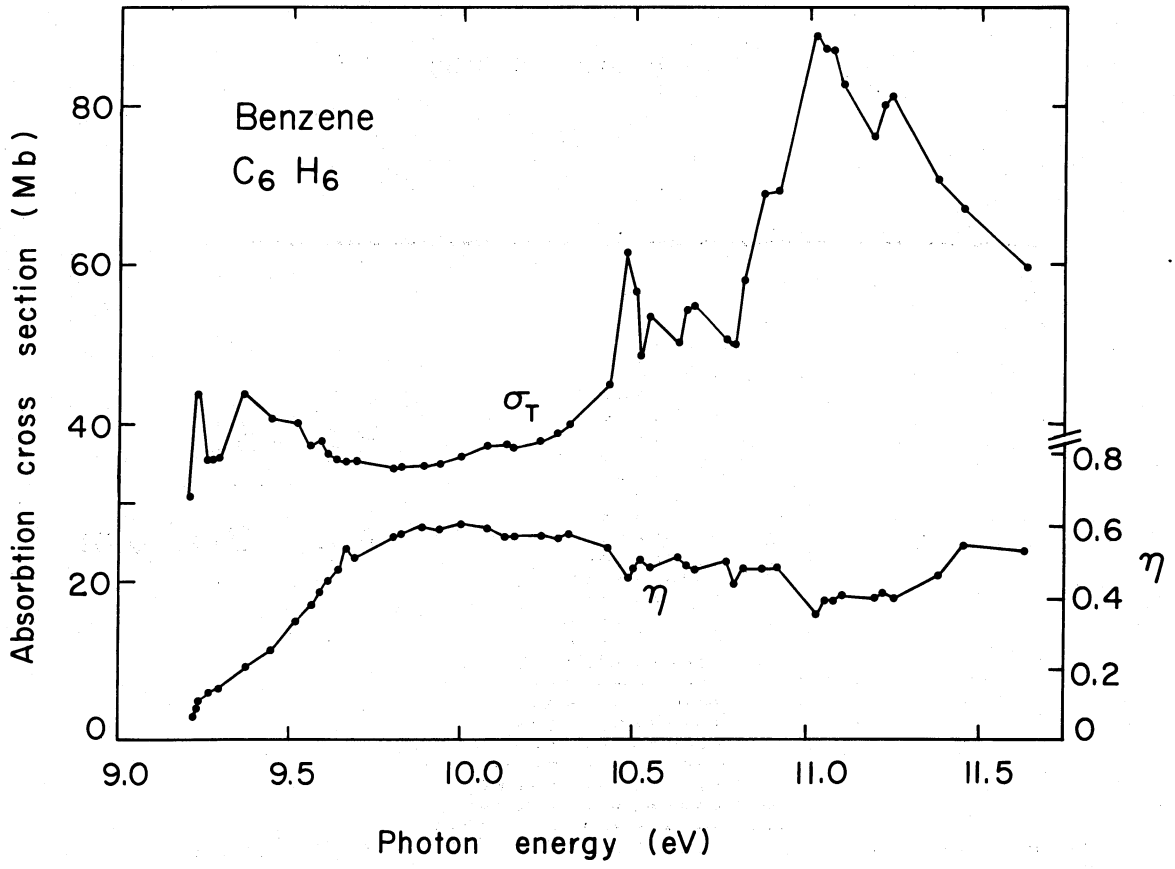
Benzene
C6 H6
σT
η
Absorbtion cross section (Mb)
80
60
40
20
0
0.8
0.6
0.4
0.2
0
η
9.0
9.5
10.0
10.5
11.0
11.5
Photon energy (eV)

Fig. 4

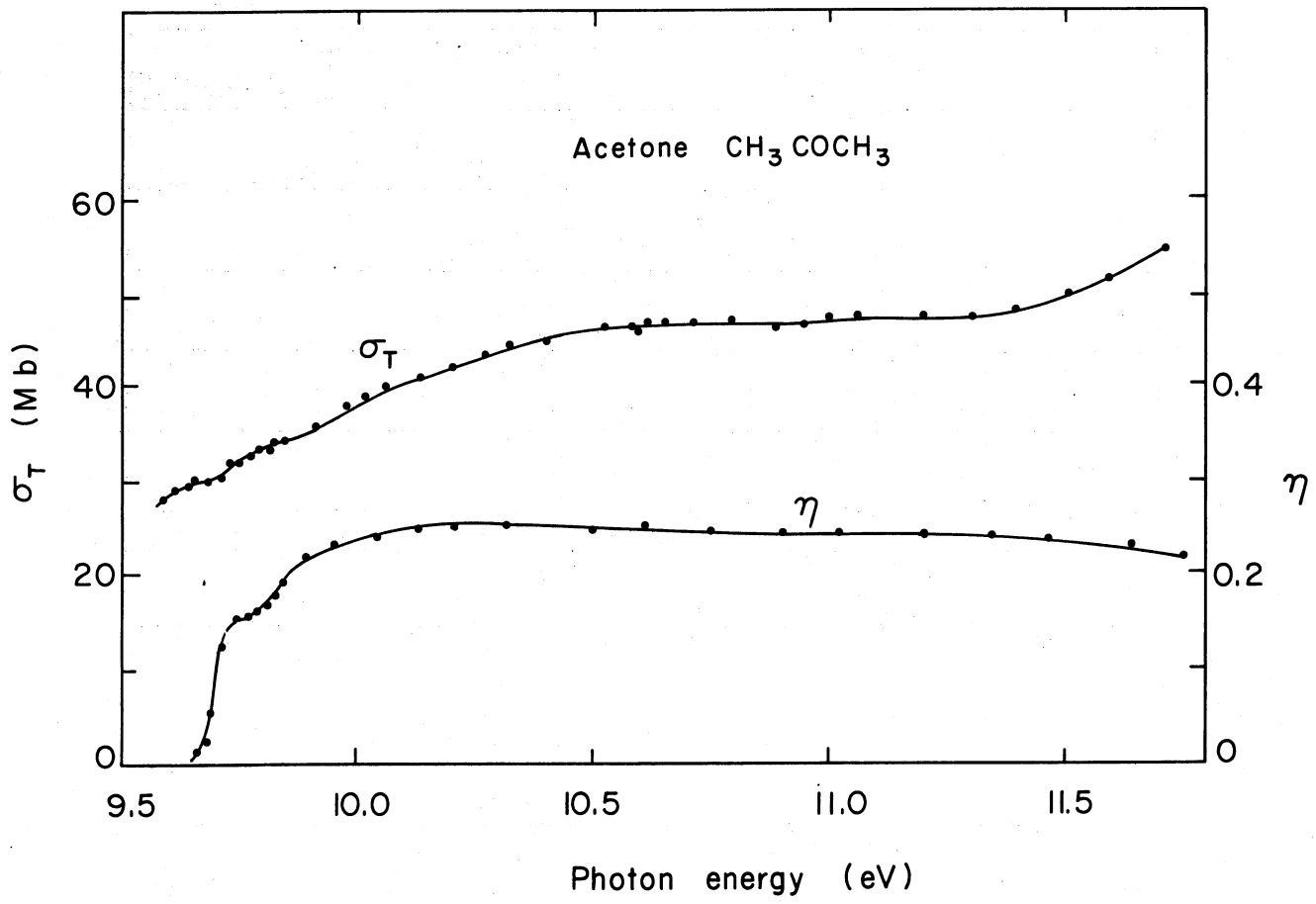
Acetone CH_3COCH_3
60
40
20
0
σ_T (Mb)
σ_T
η
0.4
0.2
0
η
9.5
10.0
10.5
11.0
11.5
Photon energy (eV)

Fig. 5

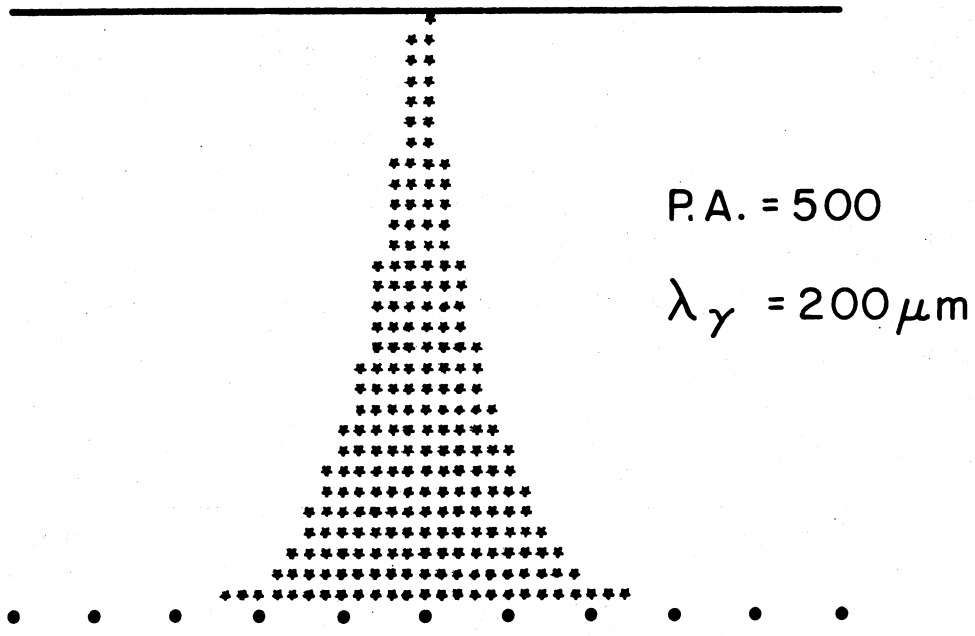
P.A. = 500
λ_γ = 200 μm

Fig. 6

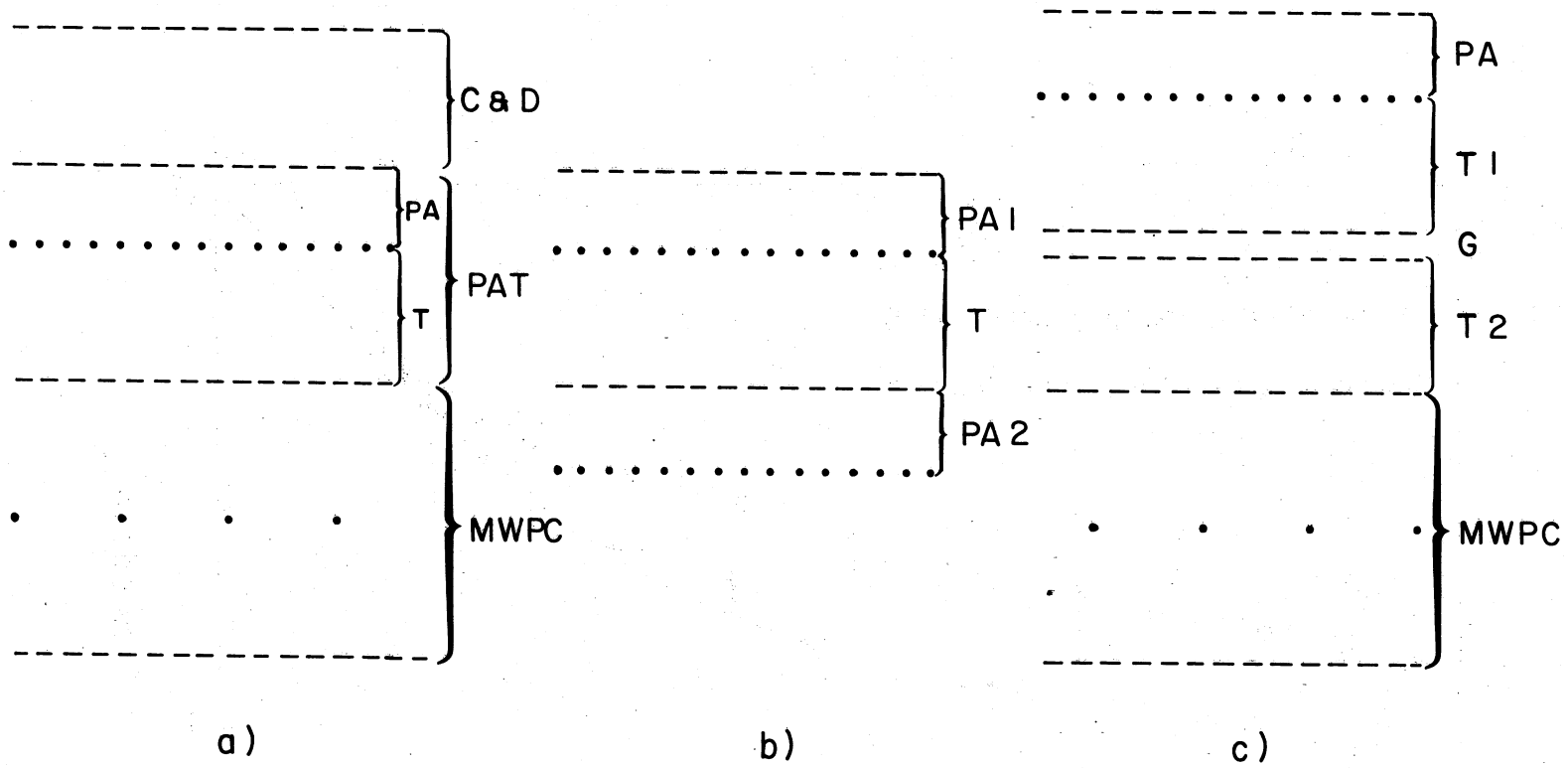

Fig. 7

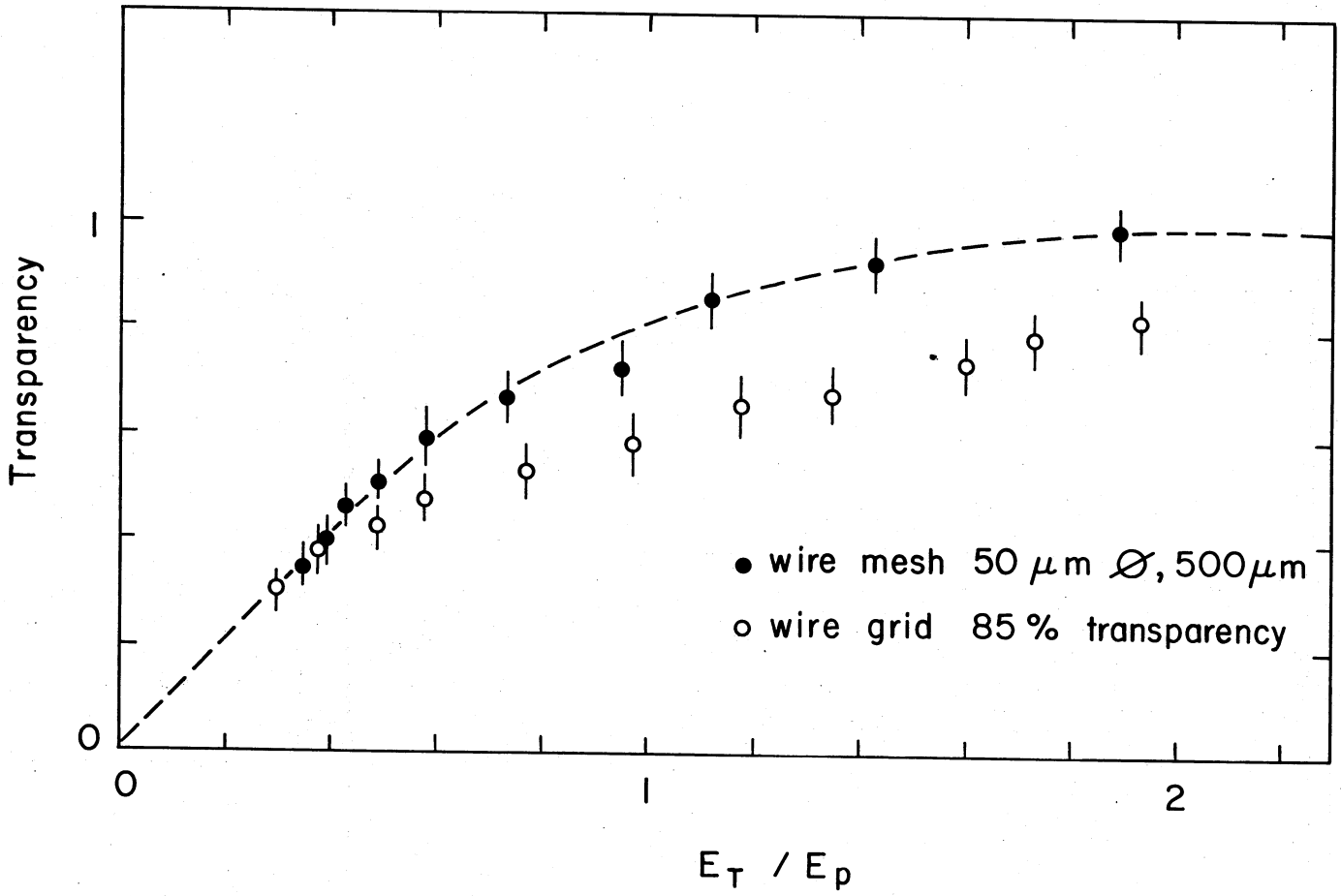
Transparency
1
0
0
1
2
E_T / E_p
● wire mesh 50 μm ∅, 500μm
○ wire grid 85 % transparency

Fig. 8

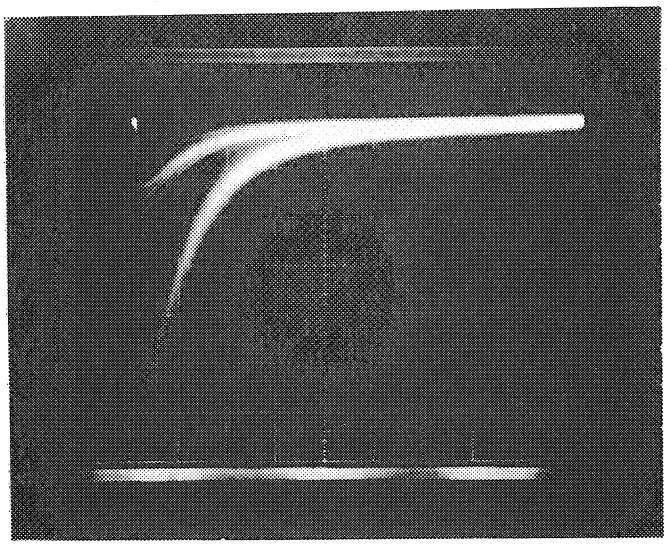

a)

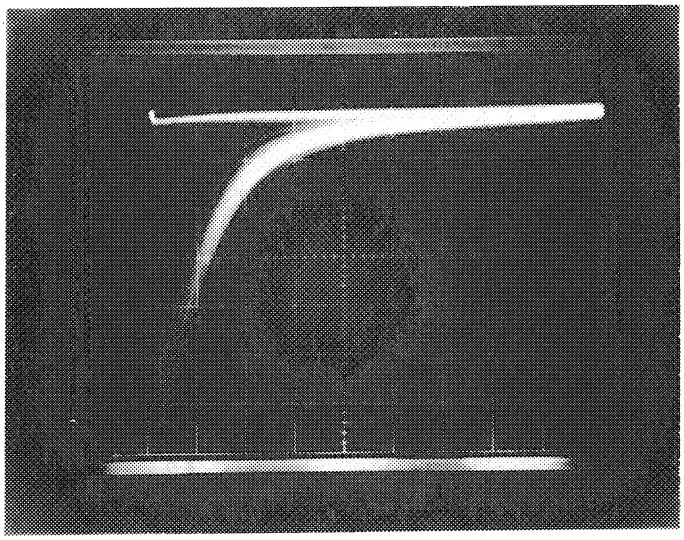

b)

Fig. 9

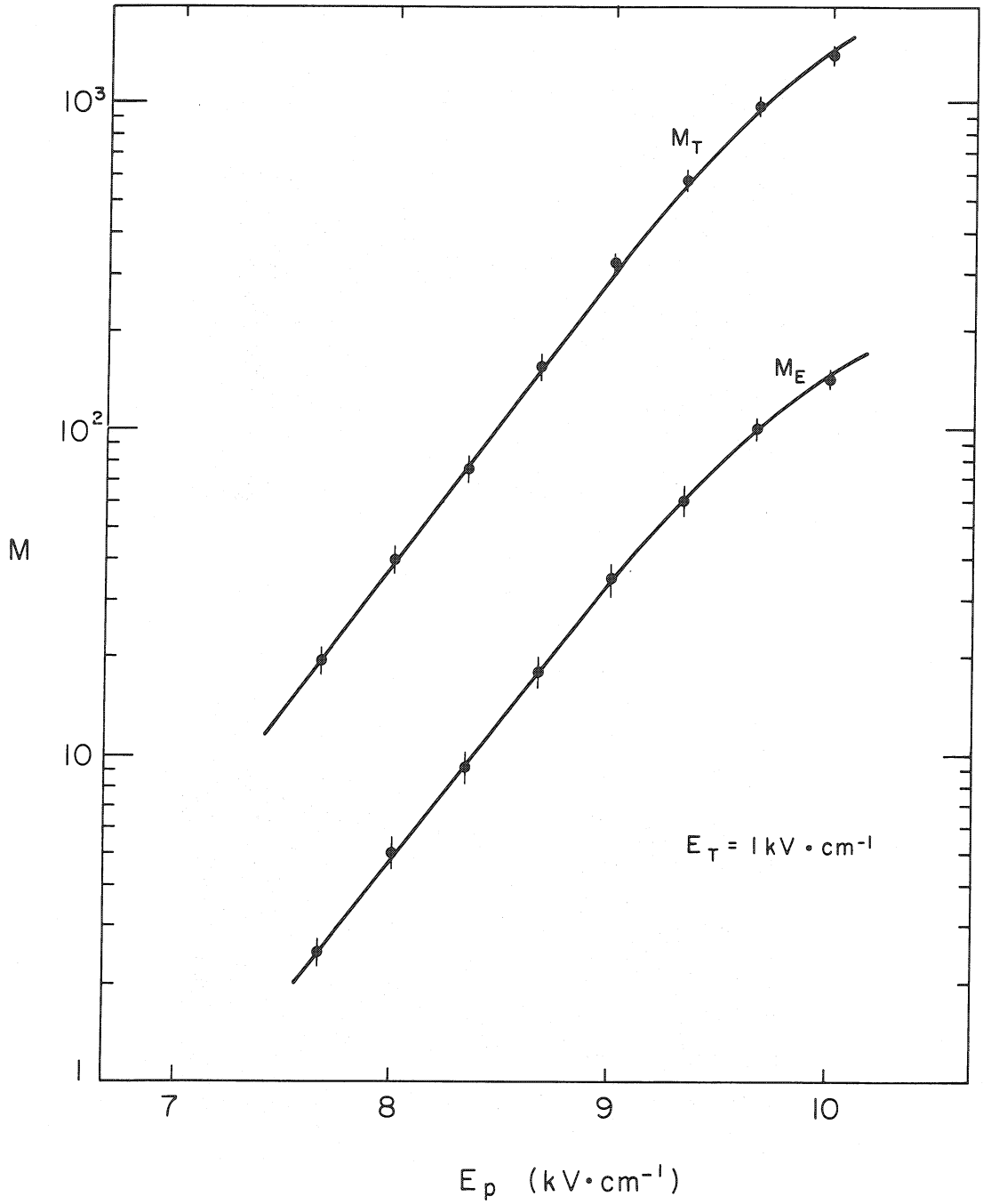

Fig. 10

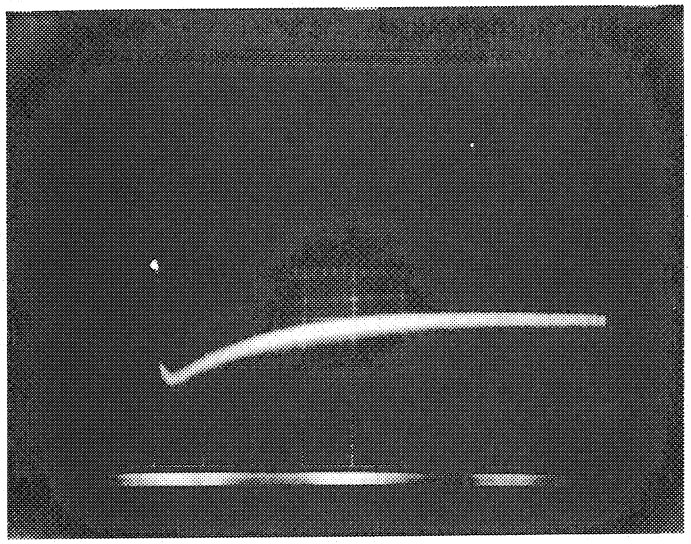

a)

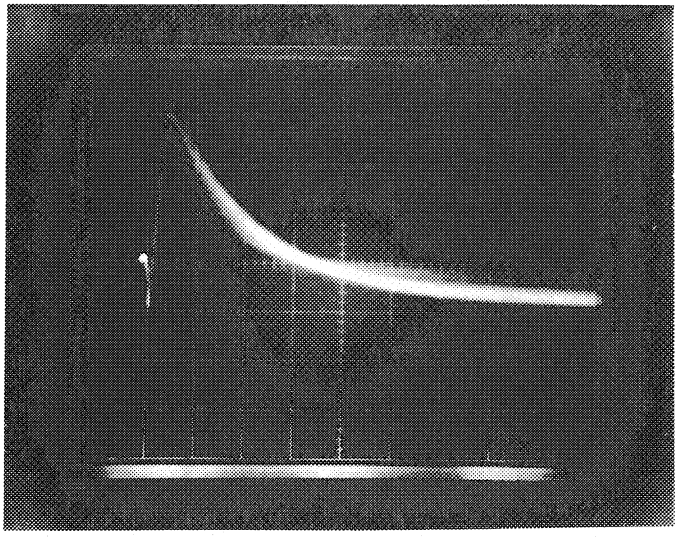

b)

Fig. 11

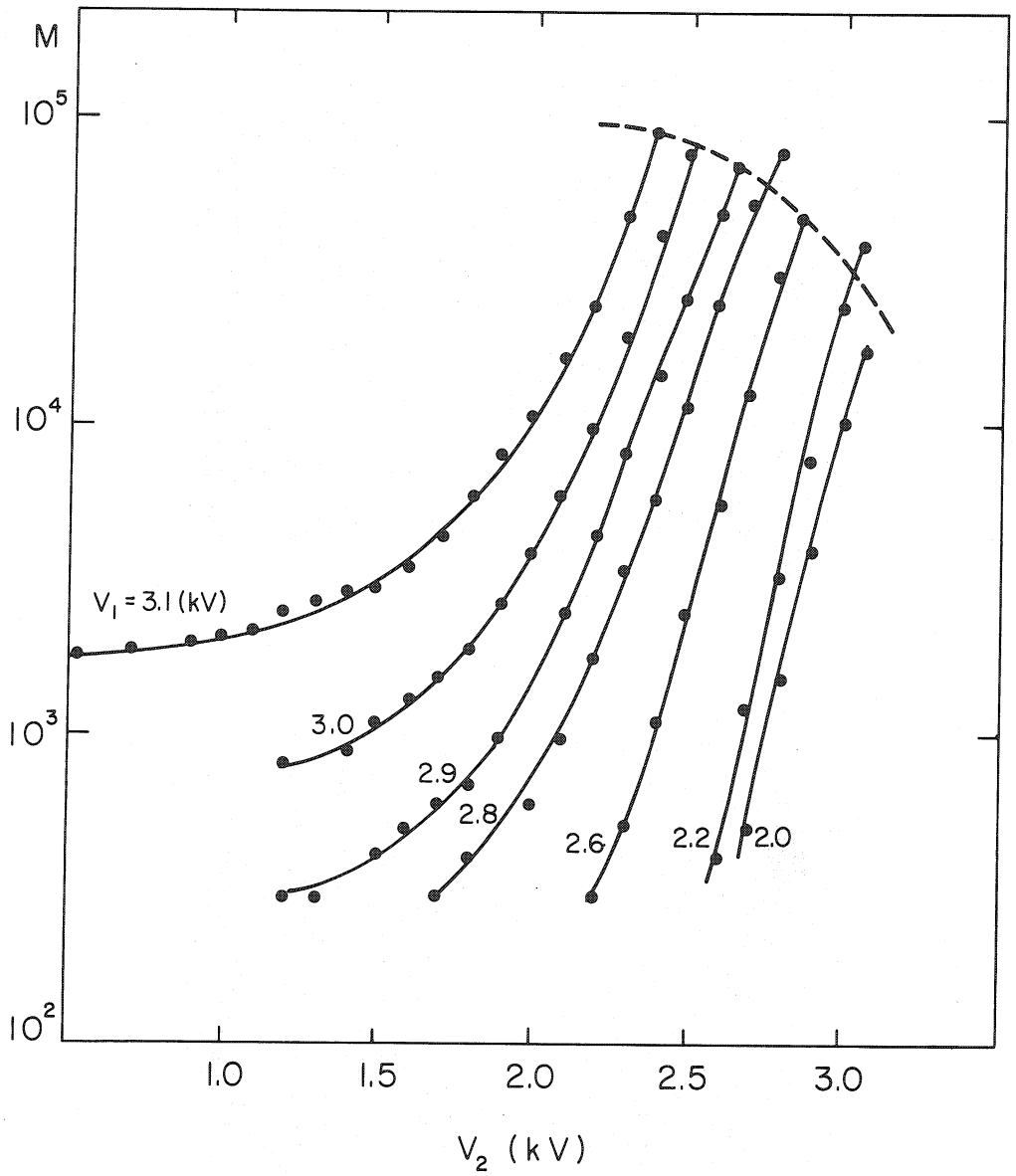

Fig. 12

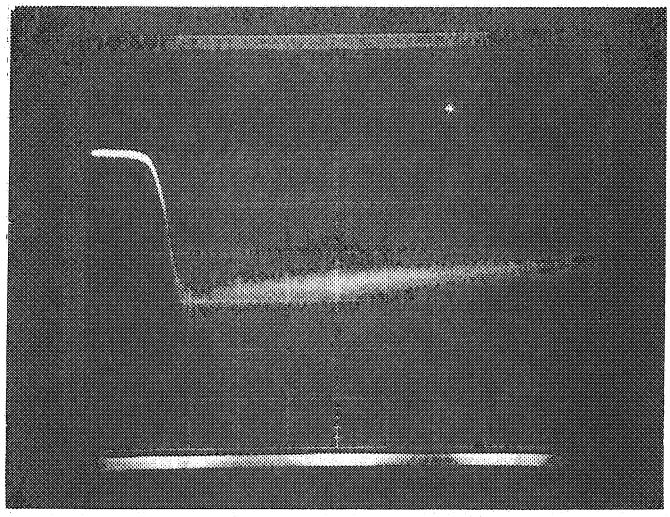

a)

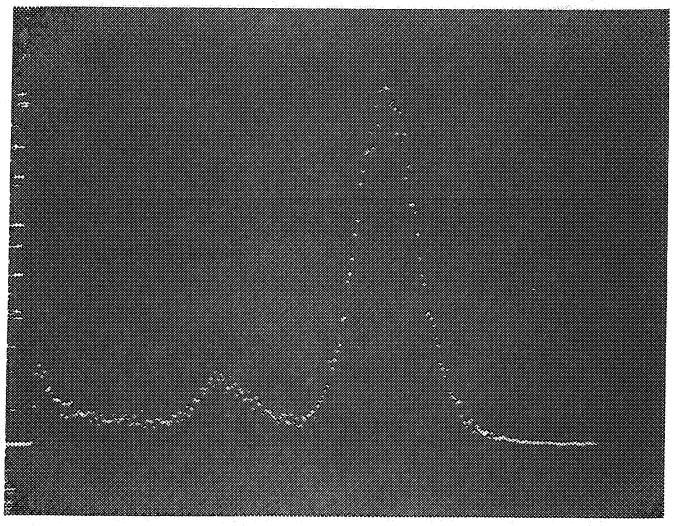

b)

Fig. 13

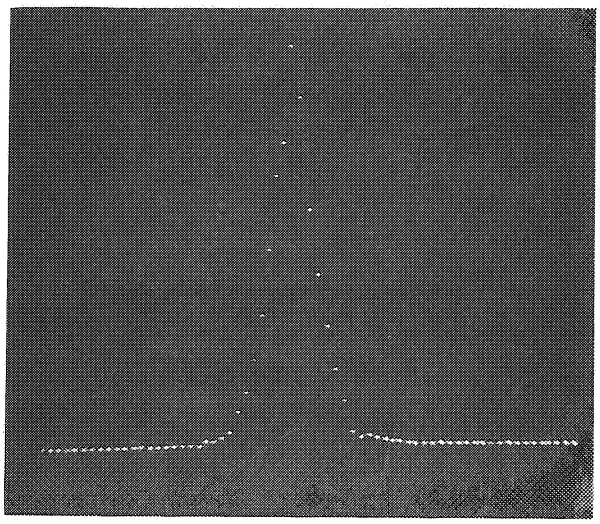

Fig. 14

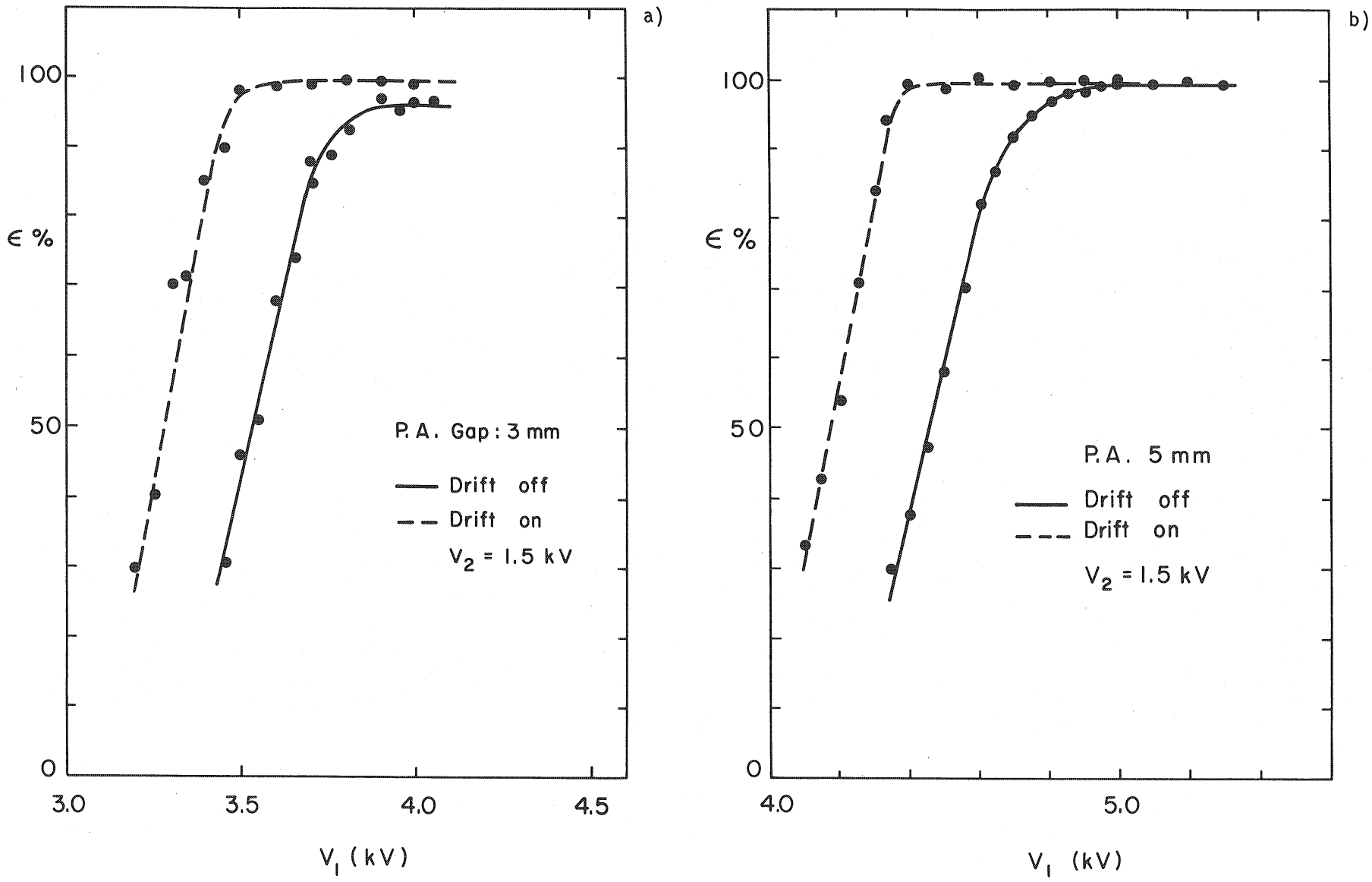
a)
100
50
0
ε %
P. A. Gap : 3 mm
Drift off
Drift on
V2 = 1.5 kV
3.0
3.5
4.0
4.5
V1 (kV)
b)
100
50
0
ε %
P. A. 5 mm
Drift off
Drift on
V2 = 1.5 kV
4.0
5.0
V1 (kV)

Fig. 15

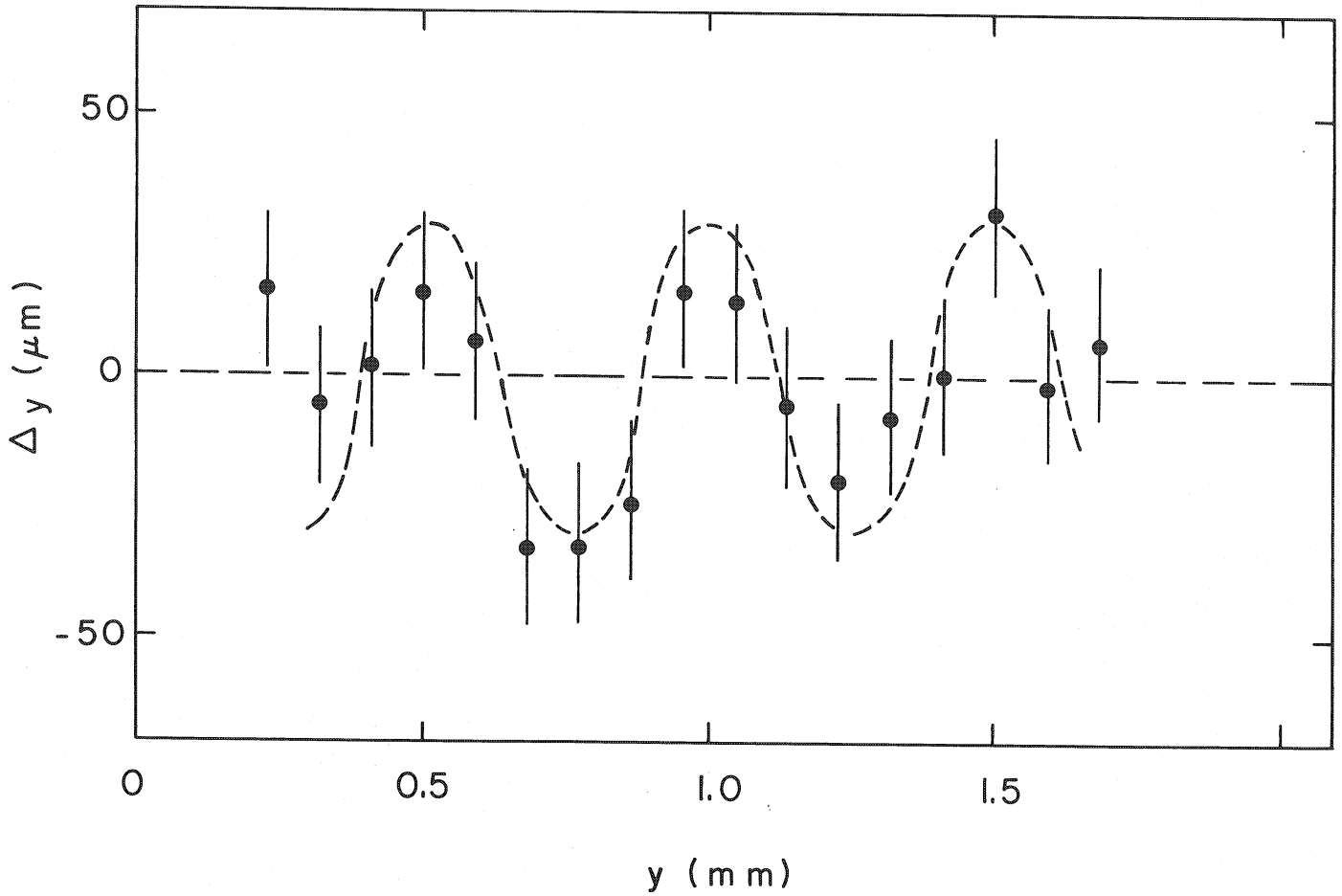

Fig. 16

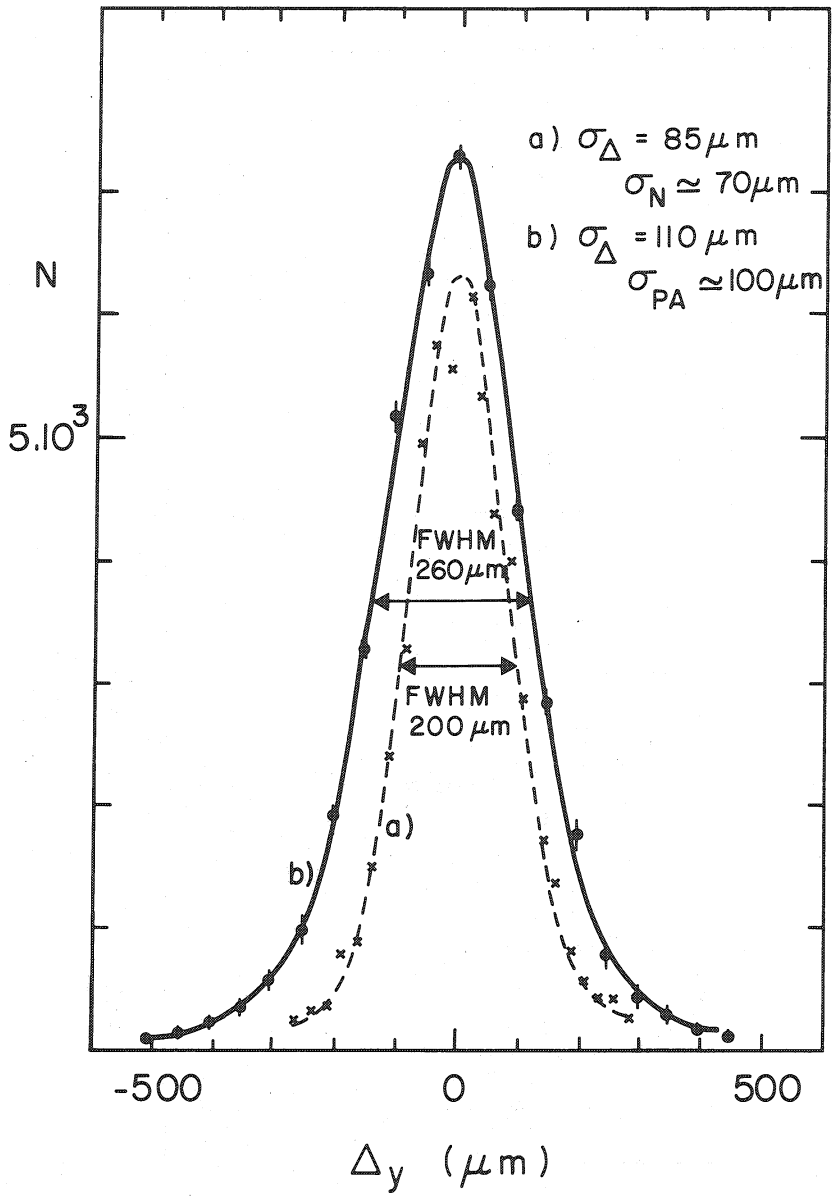
a) σ_Δ = 85 μm
$\sigma_N \simeq$ 70 μm
b) σ_Δ = 110 μm
$\sigma_{PA} \simeq$ 100 μm
N
5.10^3
FWHM
260 μm
FWHM
200 μm
a)
b)
-500
0
500
Δ_y (μm)

Fig. 17

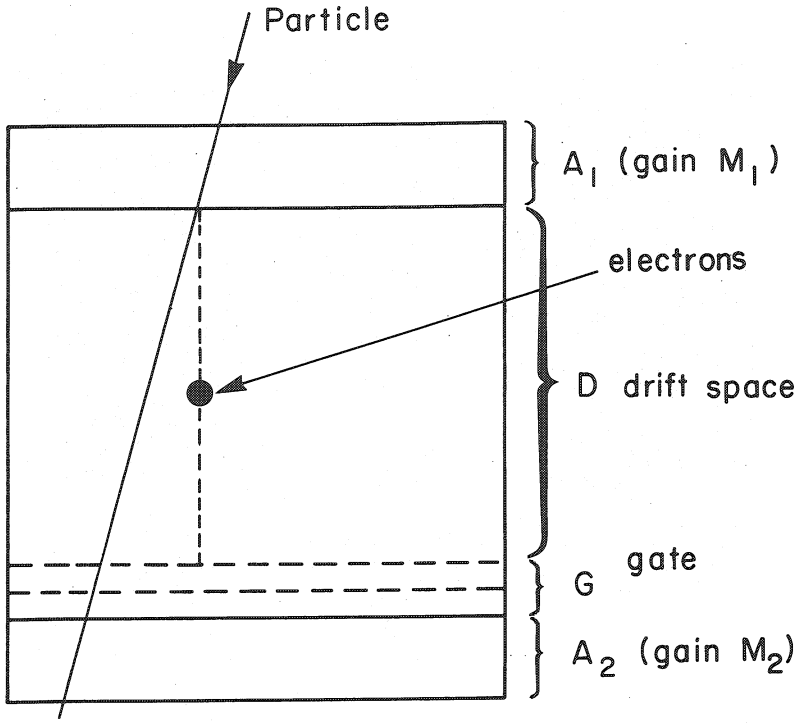

Fig. 18

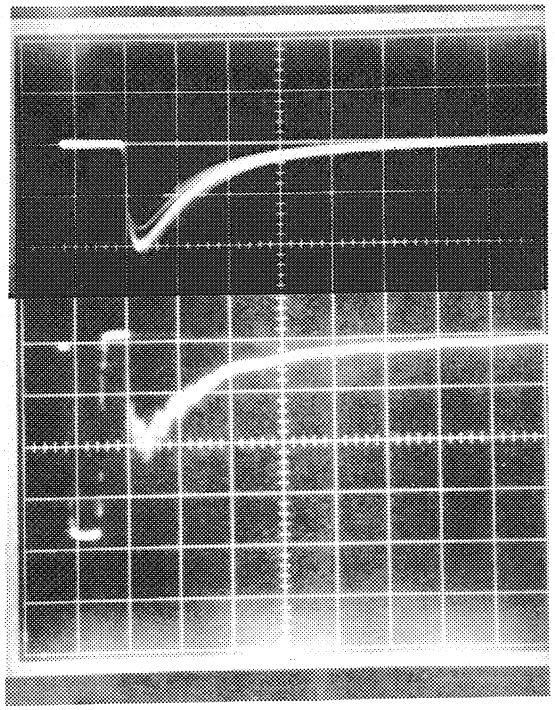

Fig. 19

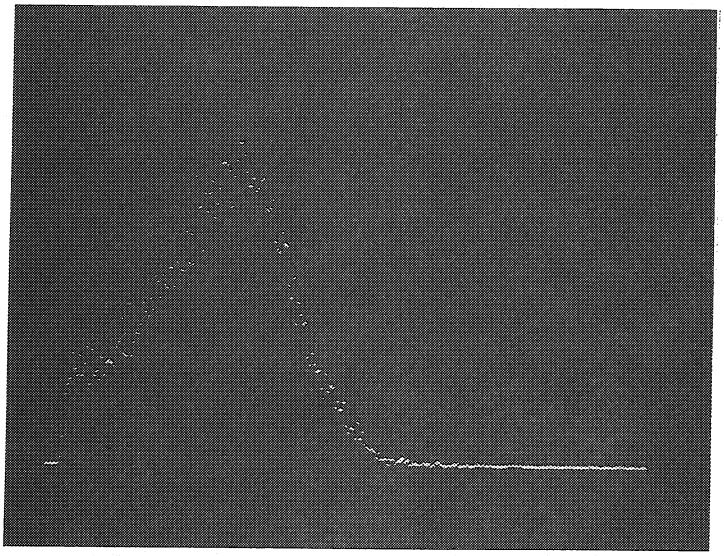

Fig. 20

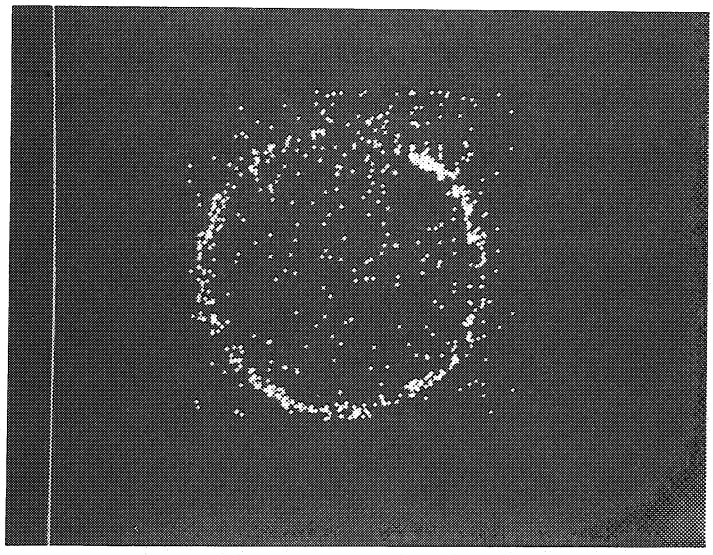

Fig. 21